Modelling the Human $Na_v1.5$ Sodium Channel: Structural and Mechanistic Insights of Ion Permeation & Drug Blockade

Supporting Information

Marawan Ahmed[1], Horia H. Jalily[1¶], Aravindhan Ganesan[1¶], Michael Houghton[2,3,4] and Khaled Barakat[1,2,3]*

[1]Faculty Of Pharmacy And Pharmaceutical Sciences, University Of Alberta, Edmonton, Ab, Canada.
[2]Li Ka Shing Institute Of Virology, University Of Alberta, Edmonton, Alberta, Canada.
[3]Li Ka Shing Applied Virology Institute, University Of Alberta, Edmonton, Alberta, Canada.
[4]Department of Medical Microbiology and Immunology, Katz Centre for Health Research, University of Alberta, Edmonton, Alberta, Canada.

*Corresponding author: email: kbarakat@ualberta.ca
¶These authors contributed equally to this work.

Detailed computational methods

1. Homology modeling of the hNa$_v$1.5 α-subunit

In the current study, the full-length amino acid sequence of the α-subunit of the human hNa$_v$1.5 (made of 2016 amino acid residues) was obtained from Uniprot database [1] (Uniprot accession code: Q14524-1). Initially, we dissected the complete sequence into nine independent sub-domains, which included four trans-membrane sub-domains and five cytoplasmic sub-domains, using the ProtParam tool [2] on the ExPASy bioinformatics resource portal [3]. Following the dissection, comparative modeling of the individual sub-domains were carried out independently using Iterative Threading Assembly Refinement (I-Tasser) [4], a robust bioinformatics program for automated protein structure prediction. We employed the existing X-ray crystal structures of the bacterial Na$_v$AB sodium channel [5] as templates for the construction of trans-membrane domains of the human hNa$_v$1.5 channel. The Na$_v$AB is a reasonable template that has been employed by many previous studies to model the 3D structures of eukaryotic VGSCs. For example, Mahdavi et al [6] used the crystal structure of Na$_v$AB (PDB ID: 3RVY) as a template to build the homology model of Na$_v$1.4. The authors relaxed the homology model with a 100 ns long classical MD simulation. Another example involves the Na$_v$1.7 channel, which was reported in a study by Yang et al [7]. The authors employed the I-Tasser software package to build the model and correlated it with several experimental observations.

Previous studies have indicated that the open state of the hNa$_v$1.5 channel bind channel's activators [8], and rarely blockers (which is the focus of the current study), such as the antiarrhythmic Flecainide [9]. On the other hand, common hNa$_v$1.5 blockers bind and

stabilize a closed state of the channel [5,10]. Therefore, we employed only the crystal structure of a closed state NaVAb (PDB ID: 3RVY) as the main template for the modeling of trans-membrane domains of hNa$_v$1.5 in this study. A sequence alignment between 3RVY and the four trans-membrane regions is given in (Figure S1), which shows the sequence identities ranging between 23% to 29%. The conservation of the overall folded structure and the presence of several conserved motifs of ion channels compensates for low-levels of identity and it has been shown previously that a sequence identity as low as 20% is sufficient to produce good quality models [11]. The long extracellular loop of DI (sequence: 276-359) was independently modeled using I-Tasser. For modeling the N-TER domain, two main templates; 4IV9 (with 19% sequence identity) and 4LDG (16% sequence identity) were used for this procedure. The best structure of the N-TER domain selected by I-Tasser following clustering was subjected to a short explicit solvent MD simulation for short MD simulations and was incorporated in the final model of the hNa$_v$1.5 structure. In addition, there were a few PDB deposited structural segments of hNav1.5 reported in the literature [12,13]. We, therefore, included these segments in our model without modifications [12,13]. One of these segments included residues 1773-1940, which was extracted from the crystal structure of the calmodulin-binding motif of the C terminus of hNa$_v$1.5 (PDB code: 4DCK) with a resolution of 2.2 Å [12]. In the same way, the inactivation gate segment composed of residues 1491-1522 was also adapted from the crystal structure of the hNa$_V$1.5 DIII-IV-Ca/CaM complex (PDB code: 4DJC) with an atomic resolution of 1.35 Å [13]. Unlike the other sub-domains in the hNa$_v$1.5 structure, the cytoplasmic region of DII (residue 417-709) and the cytoplasmic region of DIII (941-1198) sub-domains did not have very good templates (homologous structures) for

modeling. Inclusion of poorly modeled domains in our model could possibly affect the overall quality of the $hNa_v1.5$ structure, therefore, eventually impacting the trans-membrane architecture, which is the most important region of the channel. Henceforth, we decided to omit these segments from our final model of $hNa_v1.5$ and plan to add them in the future in a separate study once suitable templates emerge in the literature for these regions. Thus, our present model of the human $hNa_v1.5$ channel in this work was constructed with a total of 1465 residues. This is topologically translated into 7 sub-domains, 4 trans-membrane sub-domains, and three cytoplasmic sub-domains. For each subdomain, top models generated by I-Tasser were further refined using the ModRefiner algorithm [14] and their secondary structural qualities were verified based on the Ramachandran plots.

Subsequently, the independent models of the trans-membrane sub-domains were assembled by superposition over the corresponding segments on the 3RVY crystal structure of the closed Na_VAb using the Smith-Waterman local alignment [15] algorithm, as implemented in the UCSF Chimera program [16]. The four trans-membrane sub-domains were assembled in a clockwise manner such that the four-fold symmetry is retained in the modeled structure. A 90% score for the secondary structure alignment and an iteration threshold of 0.5 Å were employed while assembling the sub-domains over the crystal structure of Na_VAb. The cytoplasmic domains were linked to the trans-membrane domains using UCSF Chimera program. Finally, three structural models of human $hNa_v1.5$ were selected. These three models were selected based on carful visual inspection related to their compliance with the known overall $hNa_v1.5$ topology and were further

refined through fragment-guided molecular dynamic simulation (FG-MD) [17] refinement. Following the FG-MD refinement, the overall structural quality of these three final models were assessed by performing Ramachandran analysis using the RAMPAGE webserver [18].

2. Molecular dynamics simulation

Following the selection of the final three human $hNa_v1.5$ models, extensive classical molecular dynamics (MD) simulations were performed to relax these models and explore their conformational dynamics. For each model, the full simulation system was prepared using the CHARMM-GUI routine for building membrane proteins [19]. The atomistic model of the $hNa_v1.5$ protein was embedded in a lipid bilayer of 1-palmitoyl-2-oleoyl-sn-glycero-3-phosphocholine (POPC), standard protonation states of titrable residues were assumed followed by careful visual inspection of the protonation states of chargeable residues at the selectivity filters, such as Asp, Glu and Lys residues to confirm their proper protonation. The lipid layers were further topped up with a layer of TIP3P water molecules and an ionic concentration of 150 mM hNaCl solution, both in the upper (15 Å thickness from the protein) and lower (20 Å thickness from the protein) regions and neutralized with counter ions. Two different ion placement routines are available in the CHARMM-GUI [19]. The first one is an advanced Monte Carlo (MC) algorithm that considers the Columbic and vdW interactions of the placed ions with other system's components that include other ions, water, protein and lipids. The second method is a distance-based algorithm that tries to minimize steric clashes between the ion and other system's components. Although the distance-based algorithm is 80 times much faster than

the MC algorithm, we decided to use the MC algorithm to get a better ion placement [19]. Protein, lipids and ions parameters were assigned using the most recent CHARMM36 forcefield [20].

Each system was then exposed to multiple stages of minimization, heating and equilibration, before starting the production simulations. At the preliminary stage, two minimization phases were carried out to obtain reasonable starting structures. In the first phase, 50,000 steps of energy minimization were carried out, in which only the lipid tails, water molecules and ions were allowed to move freely and the rest of the system were heavily restrained to their original positions. This step ensured the removal of any severe steric clashes that may have resulted from the improper wrapping of the membrane around the protein. In the next minimization phase, the entire system was constrained with 100 kcal/mol force constant and was energy minimized for 25,000 steps. The heavy constrains on the system were gradually reduced in the three subsequent minimization cycles, from 100 kcal/mol→50 kcal/mol→ 5 kcal/mol→ 1 kcal/mol, with each minimization cycle performed for 25,000 steps. Following that, each system was slowly heated to 310 K for 5 ns and using a 1 fs integration time step, with the restrains retained at 1 kcal/mol on the protein backbone. Next, the system was equilibrated with a much-reduced restraint of 0.5 kcal/mol on the protein backbone and in two 10 ns simulations; the first simulation was run with a 1 fs time step and the later with a 2 fs time step. Finally, the production simulation was performed for approximately 680 ns, was light constrains of 0.1 kcal/mol on the trans-membrane region only employed for the first 200 ns. The Langevin thermostat [21] and an anisotropic pressure control were used to keep the temperature at 310

K and the pressure at 1 bar, respectively. A 12-Å cutoff was used to calculate the short-range electrostatic interactions and the Particle Mesh Ewald summation method was employed to account for the long-range electrostatic interactions. The NBFIX correction term was used for describing the interactions between the sodium ions and the charged carboxylate groups [22]. All simulations were carried out using NAMD 2.9 on a powerful Blue Gene\Q supercomputer [23].

3. Theoretical background of SMD

In the SMD simulation, a dummy atom was attached to the center of mass of the sodium ion using a virtual spring (with a spring constant of *k*) that is subsequently pulled with a constant velocity (*v*) and in a selected direction ($\vec{n}$). The numerical value of the pulling force at a given time ($F(t)$) can be estimated as follows,

$$F(t) = k[vt - (\overrightarrow{r_x} - \overrightarrow{r_0}).\vec{n}] \quad (1)$$

Here, *t* denotes the simulation time in pico seconds (ps), $\overrightarrow{r_x}$ is the current position of the ion and $\overrightarrow{r_0}$ is the previous position of the ion. In this study, the artificial force was applied on the ion in order to pull the ion out of the central cavity, in the direction ($\vec{n}$) of the four S6 helices of the domains (DI-DIV) into the bulk-water (where the intra-cellular environment is present *in vivo*).

SMD is one of the solid methods that has been successfully applied to understand several biological processes,[24-31] including but not limited to, ligand association/dissociation to

proteins and passage of ions from/to the ion channels [26,29,31]. For example, SMD simulations have been useful to reveal the knock-off mechanisms in potassium ion channel, through which the potassium ion migrated from the central cavity of the channel into the extracellular environment [29]. Another very recent study employed SMD approach to reveal the mechanisms of ion exchange from the extracellular environment into the central cavity of the $hNa_v1.4$ ion channel [31]. In a similar nature, Giorgino and Fabritiis [26] have employed SMD to understand the mechanisms of ion permeation (potassion ion) through gramicidin A. Thus, SMD can be a very useful computational tool to unravel the most intricate molecular details that are sometimes not fully accessible with regular MD method or by experiments.

Selection of parameters for SMD:

To select the optimal values for the constant velocity (v) and the spring constant (k), we carried out several trial simulations with the following combinations: (1) force constants, k = 1 kcal/mol/Å, 2 kcal/mol/Å, 3 kcal/mol/Å, 4 kcal/mol/Å, 5 kcal/mol/Å and (2) constant velocities, v = 0.25 Å/ps, 0.3 Å/ps, 0.35 Å/ps, 0.4 Å/ps, 0.45 Å/ps, 0.5 Å/ps. That is thirty different simulations which identified k = 4 kcal/mol/Å and 5 kcal/mol/Å in combination with v = 0.45 Å/ps as the optimal choices for the current SMD study.

4. MM-GBSA Binding Energy Calculations

Following docking, the 7 best-scoring poses for each ligand were selected for carrying out short constrained MD simulations. In order to save the computational cost and to speed up the calculations, we did not include the lipid bilayers in these simulations. This is acceptable as at this short time scale the channel is expected to preserve its overall

conformation and only the orientation of the residues interacting with the bound molecule can change slightly to accommodate the bound ligand. Our group has previously employed a similar approach for the hERG ion channel [32]. To prepare these complexes, we followed a standard protein system preparation and setup using the AMBER software package [33]. Each protein-ligand complex was immersed in a 12 $Å^3$ sized cubic box of TIP3P water molecules and the parameters for the amino acids and ligand molecules were assigned using the AMBER-FF99SB force field and the GAFF force field, respectively. Ligand charges were calculated and fitted to the atomic centers using the AM1-BCC method in antechamber. Each system was then subjected to four consecutive steps of constrained energy minimization, in which the constraints were gradually reduced in the following order: 100 → 50 → 5 → zero kcal/mol.

In each system, the protein and ligand were constrained to their reference positions using a 5 kcal/mol of force and slowly heated to 300 K over 50,000 steps. The systems were then equilibrated for 20,000 steps, where the heavy atoms of the protein and ligand were constrained with a force constant of 1 kcal/mol in the first 10,000 steps and 0.1 kcal/mol in the last 10,000 steps. Final equilibrations were carried out for 25,000 steps while retaining the constraints only on the heavy atoms of protein, but with a much reduced force constant of 0.1 kcal/mol. Later, four 250 ps production simulations with 0.1 kcal/mol constrains on the protein backbone, thus a total of 1 ns simulation, were performed for each system, which has been shown to be an efficient approach in making reliable binding free energy predictions [34]. All simulations were carried out using periodic boundary conditions and with an NPT ensemble. Short-range electrostatic interactions

were truncated after 9 Å and long range electrostatic interactions were calculated using the Particle Mesh Ewald summation. An integration time step of 1 fs was used. For each system, the binding energies were computed using the popular MMGBSA module of AMBER over the 1 ns production simulation and using a 4 ps frame separation interval [35].

5. Comparison of SMD force profiles and ion permeation in snap2 and snap4 against snap1:

SMD simulations found that the sodium ion trapped at the central cavity in two other structures, snap2 (Figure S6) and snap4 (Figure S7), also released via pathway 1. Nevertheless, the orientations of P1/P2 turns of DIII and P1 helix of DII in snap2 and snap4 are significantly different when compared to those in snap1. Especially, in snap2, the P1 helix of DII moved significantly towards the left-side, such that some of the residues in this helix (F892 and C896, for example) were oriented towards the central cavity, thereby constricting the space for the forward movement of the sodium ion in the direction of pathway 1. Hence, it can be noted that the force profile of snap2 (in Figure S6) displays two short peaks reaching ~600 pN at < 20 ps, which relates to breaking of the interactions of sodium ion with the DEKA residues, moving across the P1 helix of DII and passing through the hydrophobic contacts of F1760 and Y1767.

Subsequently, as in the case of snap1, the force in the force profile of snap2 also gradually increased to ~1200 pN between 25-60 ps, which was essential to break the stacking of F1459 and F934 and N1463-L938 H-bond interactions. The number of water molecules coordinating with sodium ion (in its first solvation shell) dropped intermittently while

breaking through these barriers, which later picked up and was stabilized between 6-7. The ion released completely from the influence of transmembrane at about 80 ps, after which the force profile remained flat until the end of the simulation. Similar processes were also found in the ion permeation in snap4 (refer to Figure S7). Thus, it is clear that the ion released through the pathway 1 (between S6 helices of DII and DIII) was controlled by four residues, F1459, F934, N1463 and L938, which act as significant gatekeepers of this tunnel.

Figure S1. Sequence alignments between the bacterial ion channel template (PDB ID: 3RVY) and the four trans-membrane domains. No good alignment was observed for the long extracellular loop of DI (276-359) and thus this loop was independently modeled using I-Tasser.

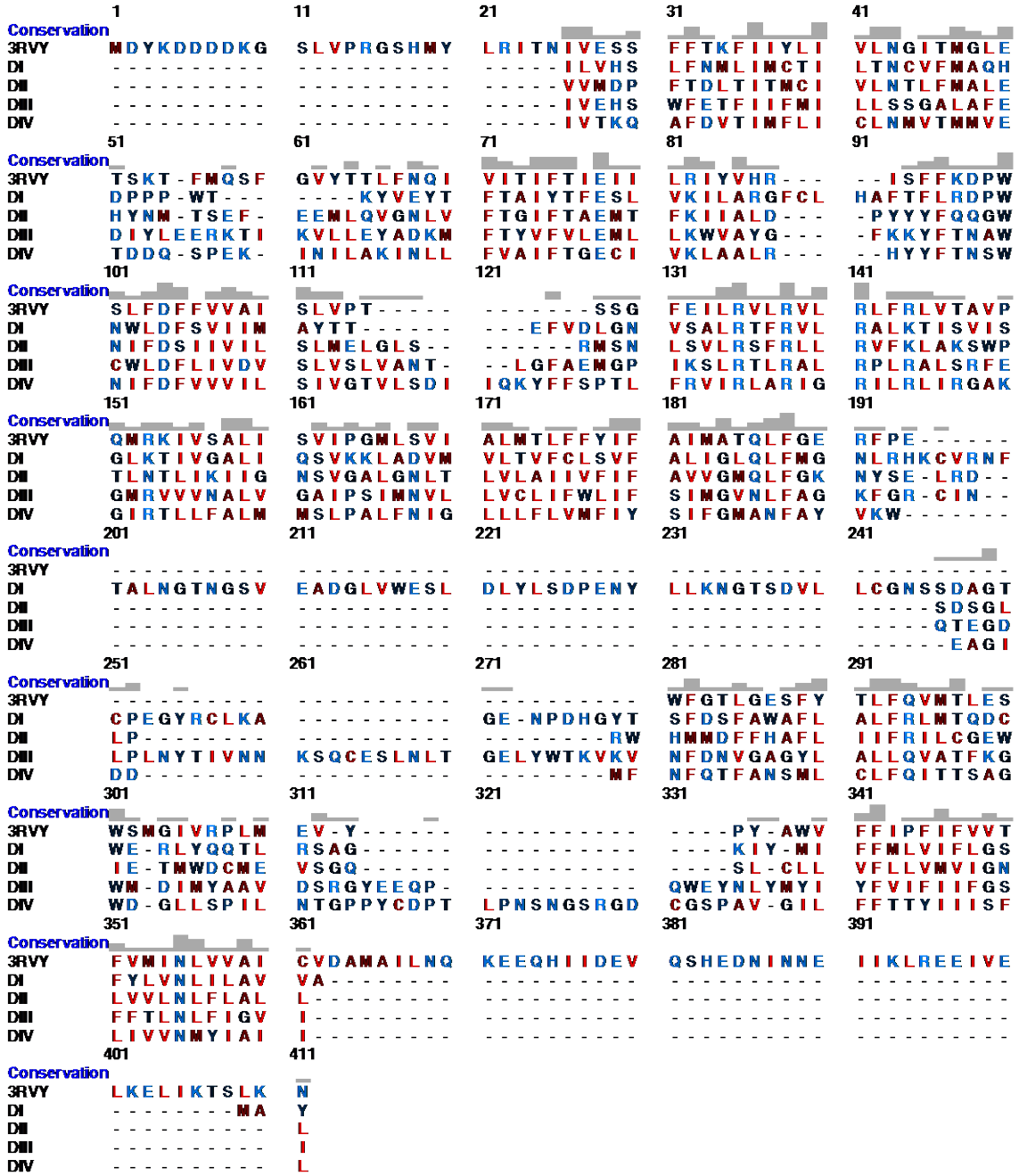

Figure S2. Ramachandran plots of the three different $Na_v1.5$ models constructed using the homology modeling approaches implemented in I-Tasser server.

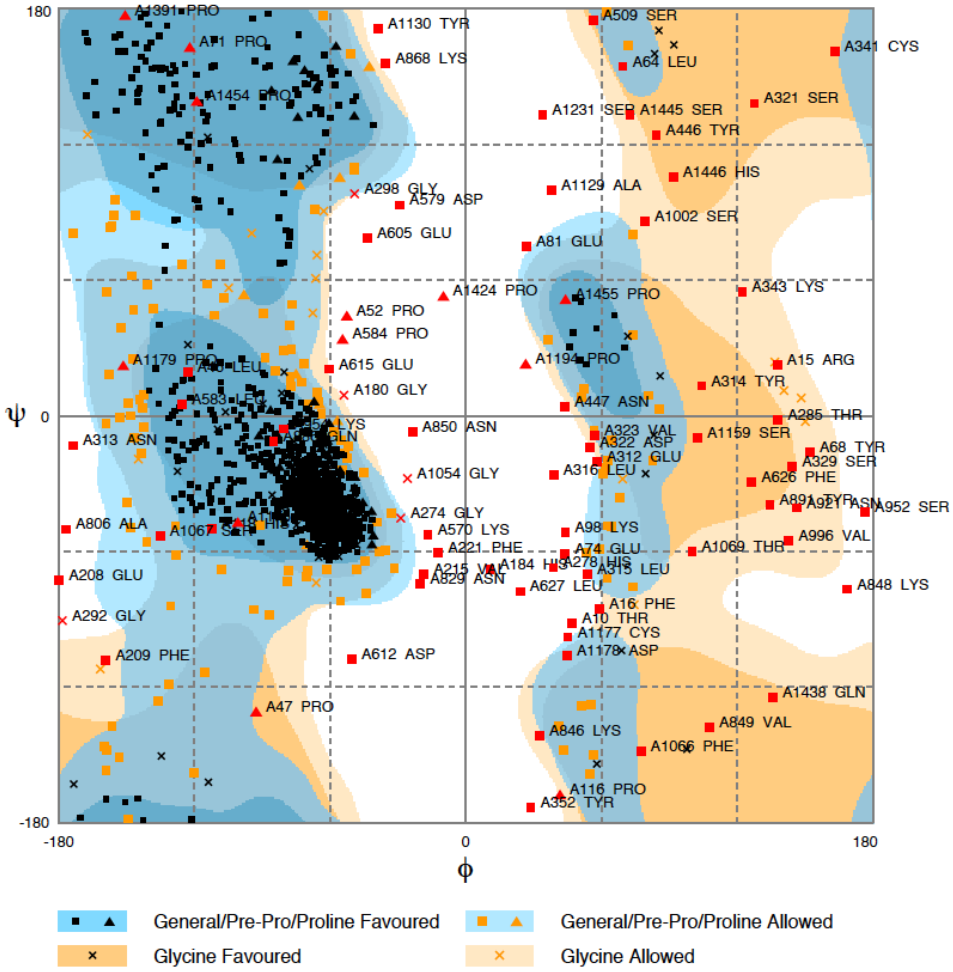

Number of residues in favoured region (~98.0% expected) : 1219 (84.2%)
Number of residues in allowed region (~2.0% expected) : 145 (10.0%)
Number of residues in outlier region : 83 (5.7%)

RAMPAGE by Paul de Bakker and Simon Lovell available at http://www-cryst.bioc.cam.ac.uk/rampage/

Please cite: S.C. Lovell, I.W. Davis, W.B. Arendall III, P.I.W. de Bakker, J.M. Word, M.G. Prisant, J.S. Richardson & D.C. Richardson (2002)
Structure validation by Cα geometry: ϕ/ψ and Cβ deviation. Proteins: Structure, Function & Genetics. 50: 437-450

Figure S2 (b): Model 2 Ramachandran statistics

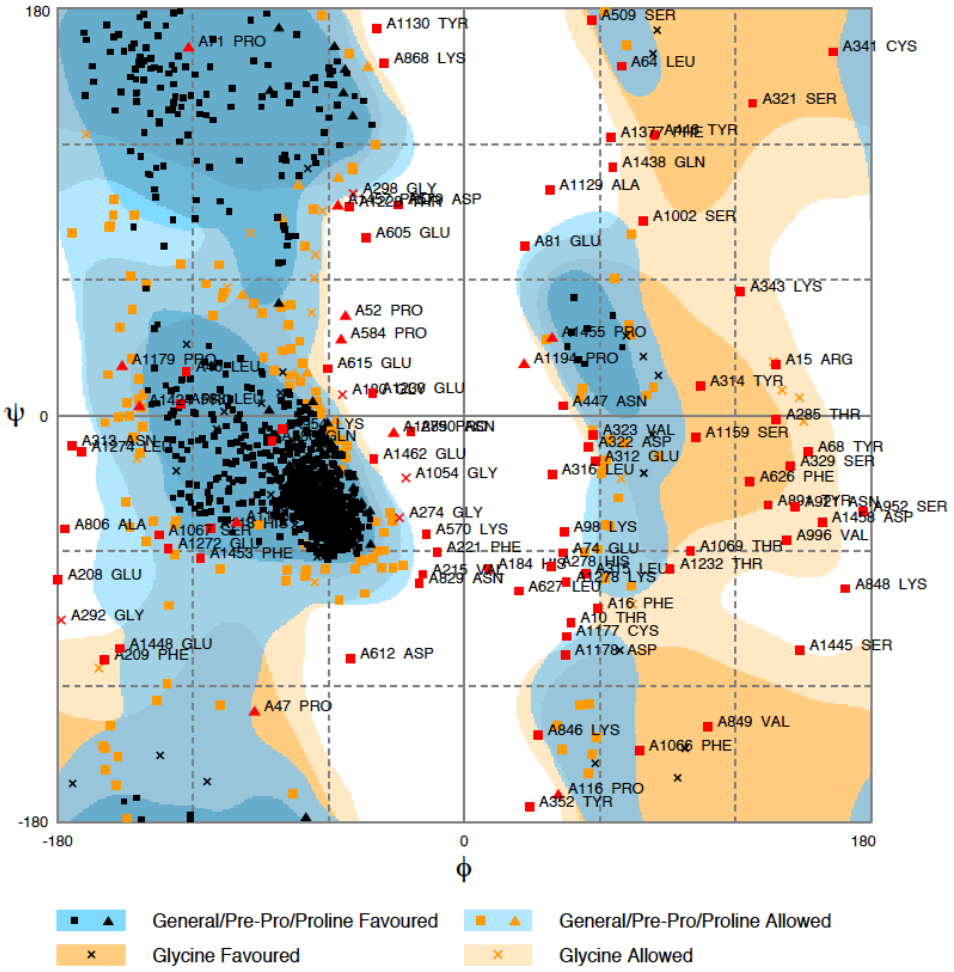

Number of residues in favoured region (~98.0% expected)	: 1201 (82.4%)
Number of residues in allowed region (~2.0% expected)	: 164 (11.3%)
Number of residues in outlier region	: 92 (6.3%)

RAMPAGE by Paul de Bakker and Simon Lovell available at http://www-cryst.bioc.cam.ac.uk/rampage/

Please cite: S.C. Lovell, I.W. Davis, W.B. Arendall III, P.I.W. de Bakker, J.M. Word, M.G. Prisant, J.S. Richardson & D.C. Richardson (2002) Structure validation by Cα geometry: ϕ/ψ and Cβ deviation. Proteins: Structure, Function & Genetics. 50: 437-450

Figure S2(c): Model 3 Ramachandran statistics

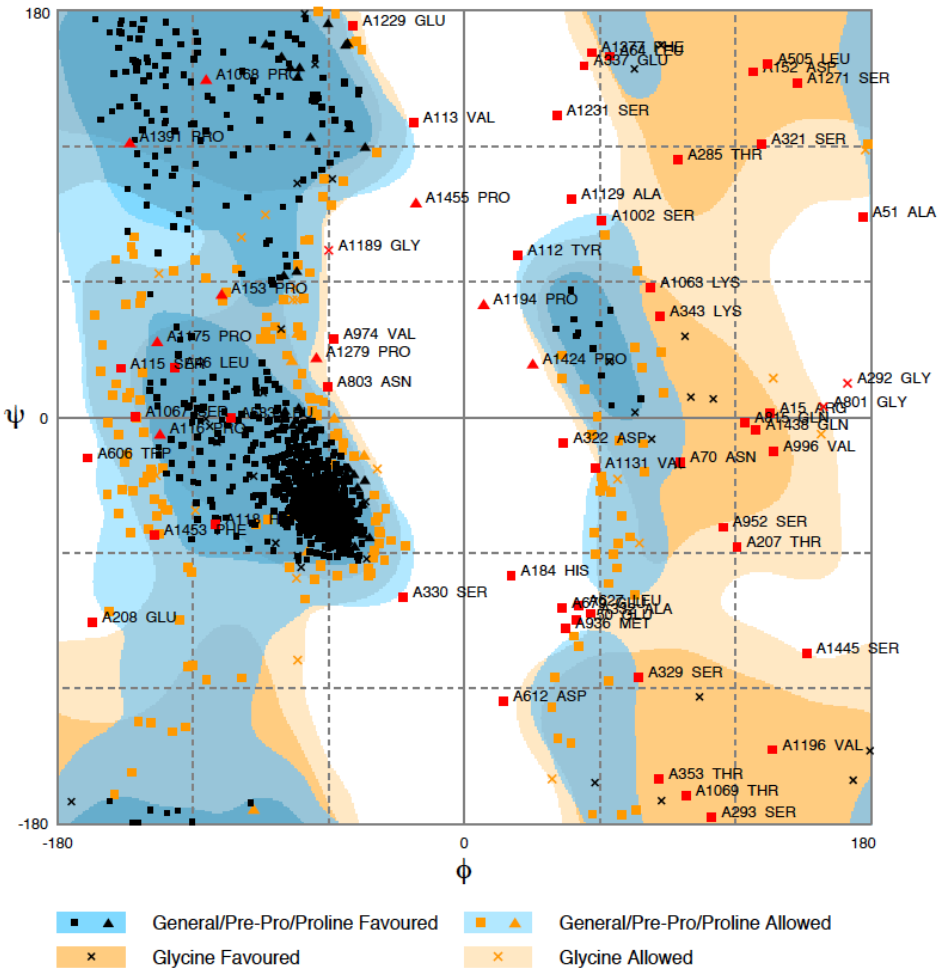

Number of residues in favoured region (~98.0% expected)	: 1210 (82.9%)
Number of residues in allowed region (~2.0% expected)	: 187 (12.8%)
Number of residues in outlier region	: 62 (4.2%)

RAMPAGE by Paul de Bakker and Simon Lovell available at http://www-cryst.bioc.cam.ac.uk/rampage/

Please cite: S.C. Lovell, I.W. Davis, W.B. Arendall III, P.I.W. de Bakker, J.M. Word, M.G. Prisant, J.S. Richardson & D.C. Richardson (2002) Structure validation by Cα geometry: ϕ/ψ and Cβ deviation. Proteins: Structure, Function & Genetics. 50: 437-450

Figure S2(d): Model 3 Ramachandran statistics (after MD)

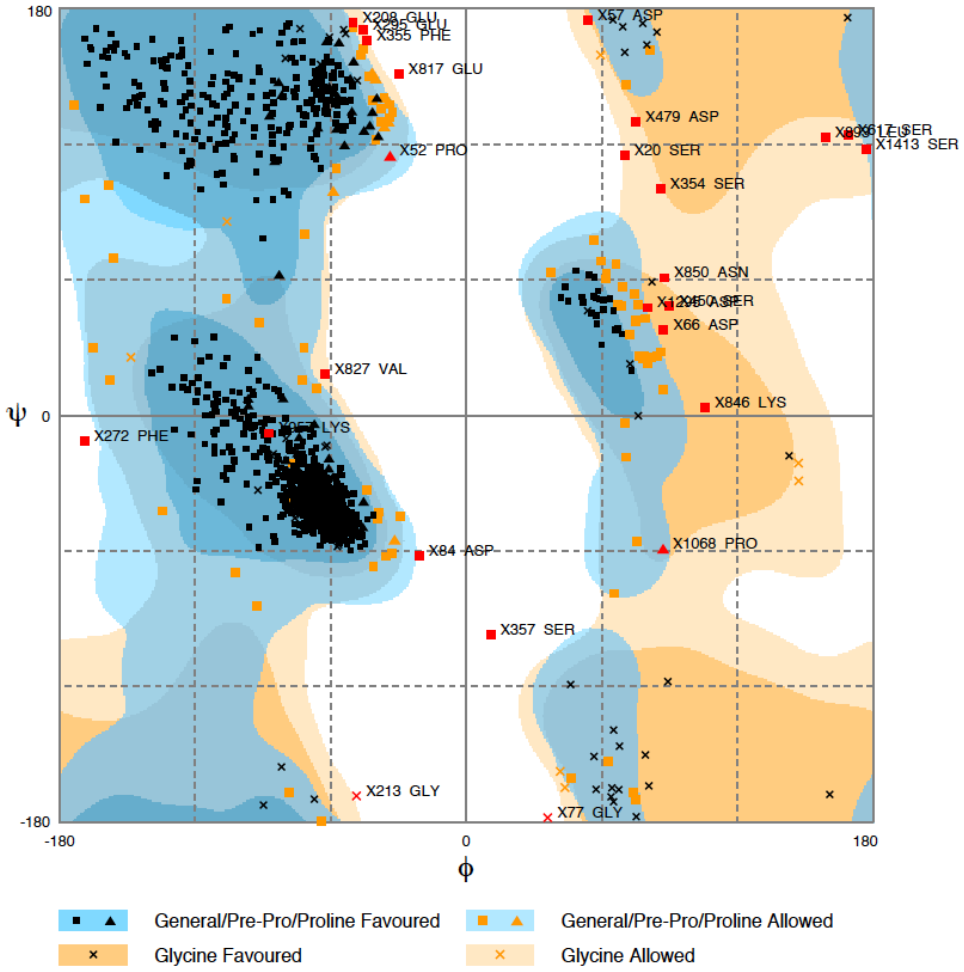

Number of residues in favoured region (~98.0% expected)	: 1293 (92.0%)
Number of residues in allowed region (~2.0% expected)	: 88 (6.3%)
Number of residues in outlier region	: 25 (1.8%)

RAMPAGE by Paul de Bakker and Simon Lovell available at http://www-cryst.bioc.cam.ac.uk/rampage/

Please cite: S.C. Lovell, I.W. Davis, W.B. Arendall III, P.I.W. de Bakker, J.M. Word, M.G. Prisant, J.S. Richardson & D.C. Richardson (2002) Structure validation by Cα geometry: ϕ/ψ and Cβ deviation. Proteins: Structure, Function & Genetics. 50: 437-450

Figure S3. A side view for the complete membrane embedded $Na_v1.5$ system used for the MD simulation. The coloring scheme is consistent with what have been given previously.

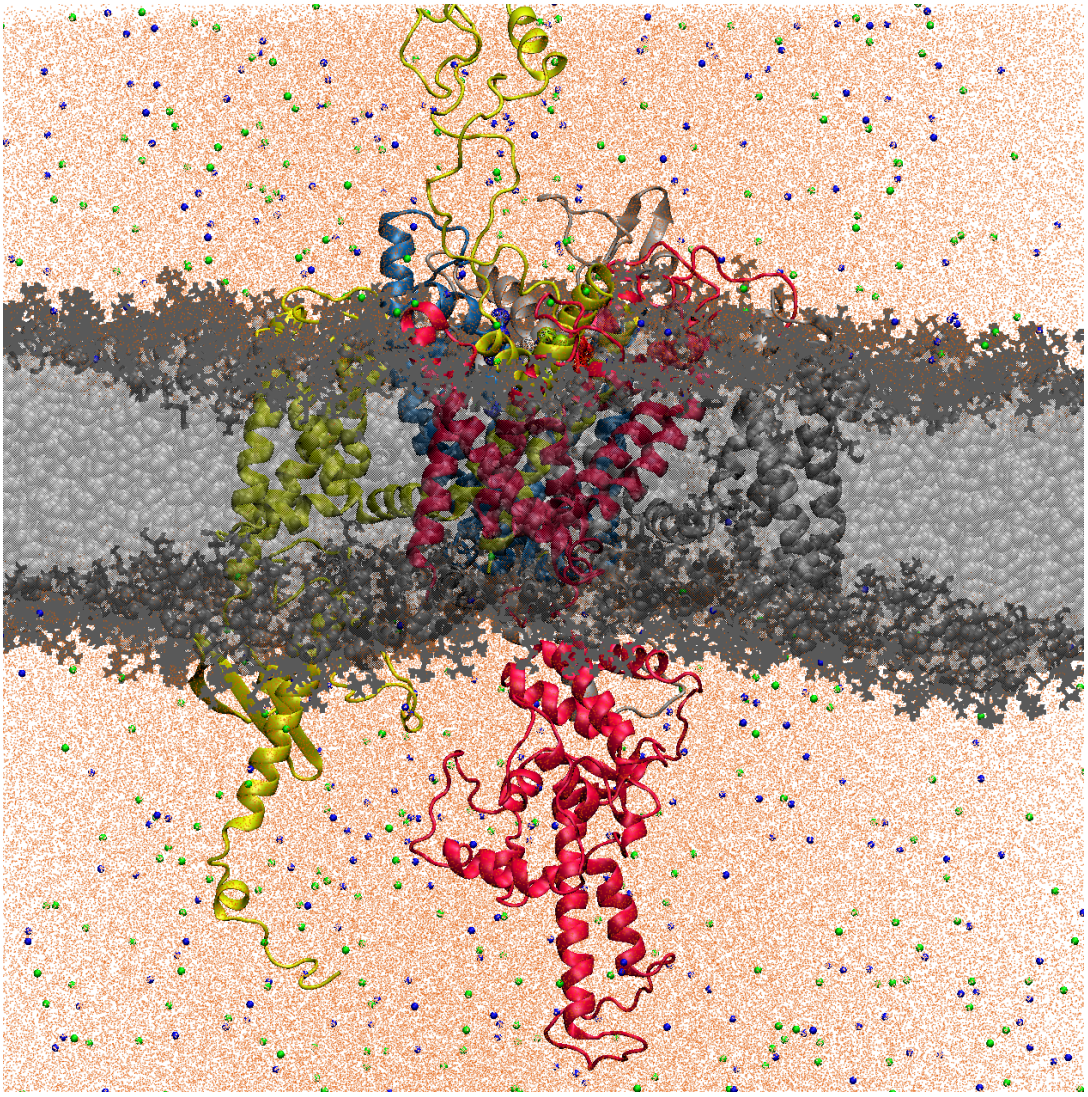

Figure S4. The atomic RMSD plot for the Cα atoms of the trans-membrane region of $Na_v1.5$ over the 580 ns MD simulation trajectory. The plot shows a stable trajectory for this fairly large simulation system.

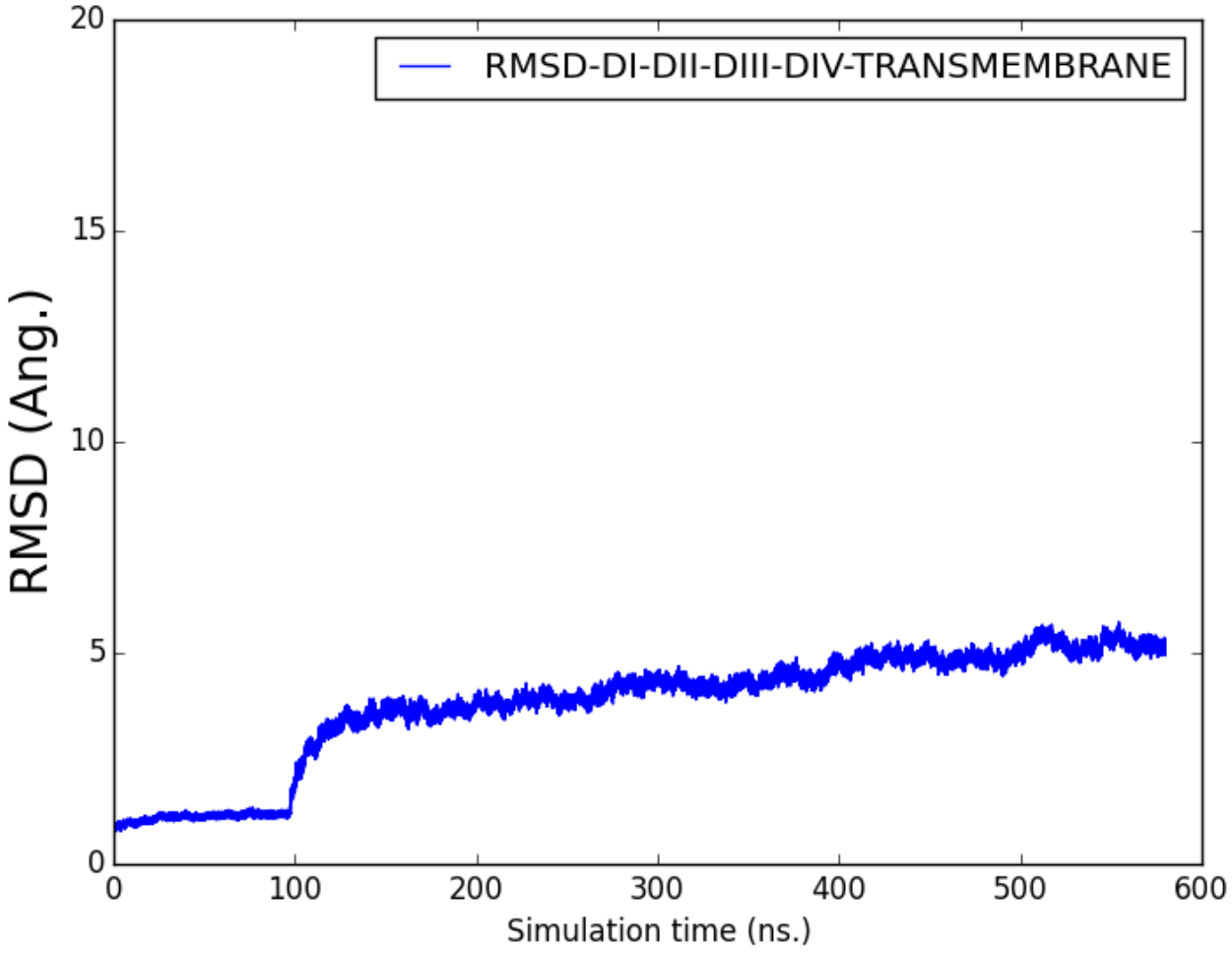

Figure S5. Time-evolution of H-bond distances between the side chain oxygen atom of N1463 and and the two hydrogen atoms of the side chain methyl groups in L938.

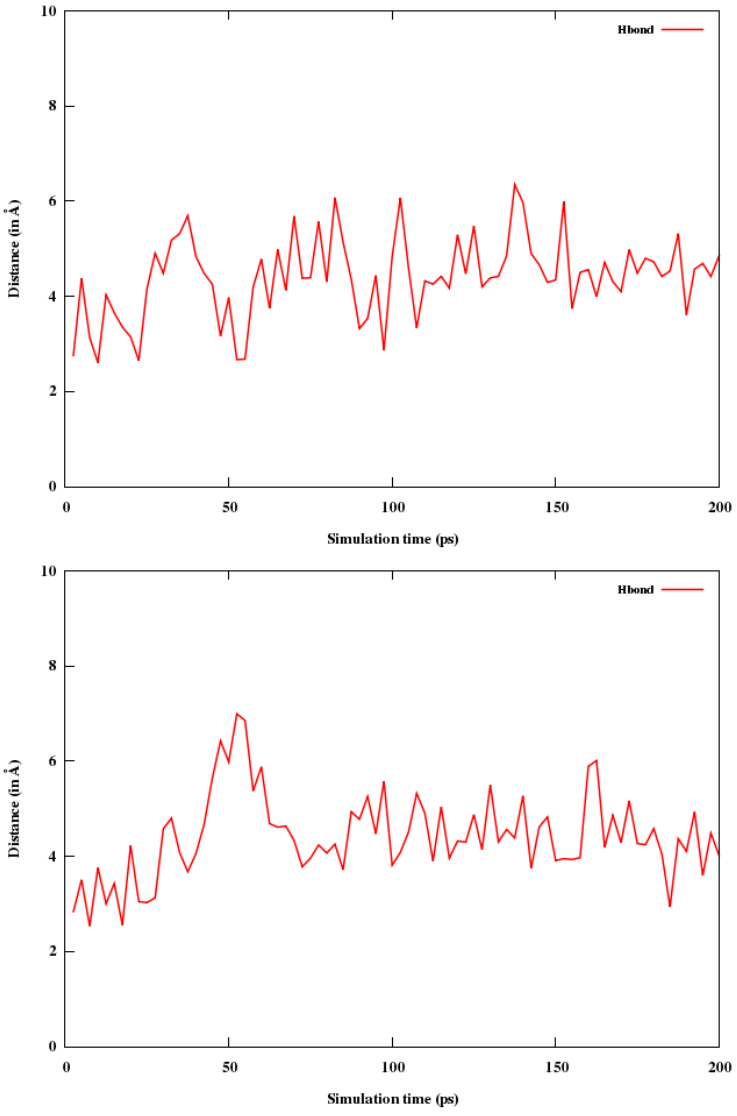

Figure S6. The pulling of Na+ ion out of the central cavity of the $Na_v1.5$ model in the final snapshot (or snap2) through pathway 1. The 3D representation on the left describes that the Na+ ion (shown as a yellow VDW sphere) trapped near the DEKA motif at the central cavity of the ion channel exiting through the S6 helices (shown as blue ribbons) of the domains, DII and DIII (pathway 1). The ion, under the influence of external force, passes through a number of hydrophobic residues (shown as sticks and listed in the figure) and finally released by the conformational changes of F934 (see within the circle) and the disruption of H-bonds between N1463 and L938 residues (shown as broken lines in black). The positions of the ion surrounded by water molecules at different timescales (*3 ps, 23 ps, 58 ps and 78 ps*) during the SMD simulation are shown as VDW spheres in yellow and the positions of the ions along each step until the release are shown as smaller CPK spheres in red. The corresponding force profile for the pulling of the ion and the numbers of water molecules surrounding the ions throughout this trajectory are shown in the bottom and the upper panels, respectively, of the right-side figure.

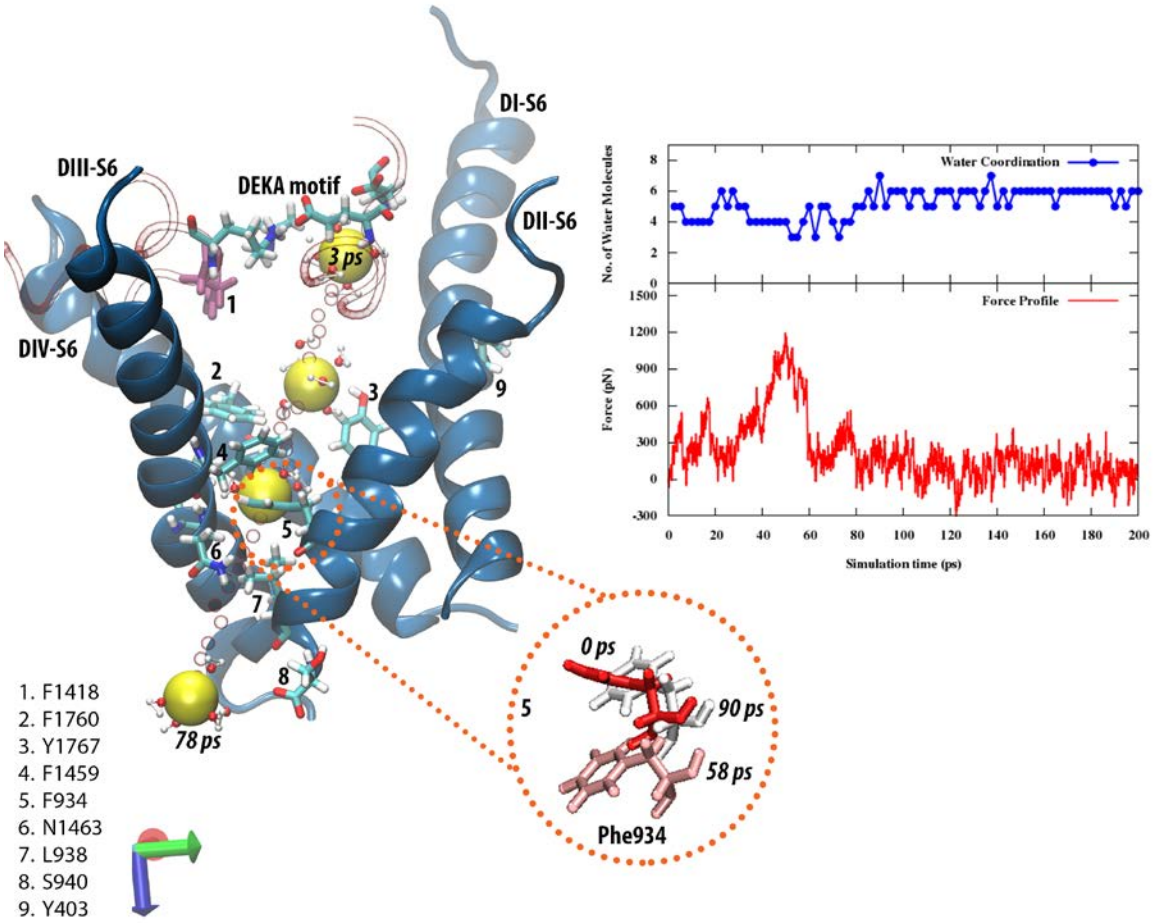

Figure S7. The pulling of Na+ ion out of the central cavity of the $Na_v1.5$ model in the final snapshot (or snap4) through pathway 1. The 3D representation on the left describes that the Na+ ion (shown as a yellow VDW sphere) trapped near the DEKA motif at the central cavity of the ion channel exiting through the S6 helices (shown as blue ribbons) of the domains, DII and DIII (pathway 1). The ion, under the influence of external force, passes through a number of hydrophobic residues (shown as sticks and listed in the figure) and finally released by the conformational changes of F934 (see within the circle) and the disruption of H-bonds between N1463 and L938 residues (shown as broken lines in black). The positions of the ion surrounded by water molecules at different timescales (*3 ps, 28 ps, 63 ps and 80 ps*) during the SMD simulation are shown as VDW spheres in yellow and the positions of the ions along each step until the release are shown as smaller CPK spheres in red. The corresponding force profile for the pulling of the ion and the numbers of water molecules surrounding the ions throughout this trajectory are shown in the bottom and the upper panels, respectively, of the right-side figure.

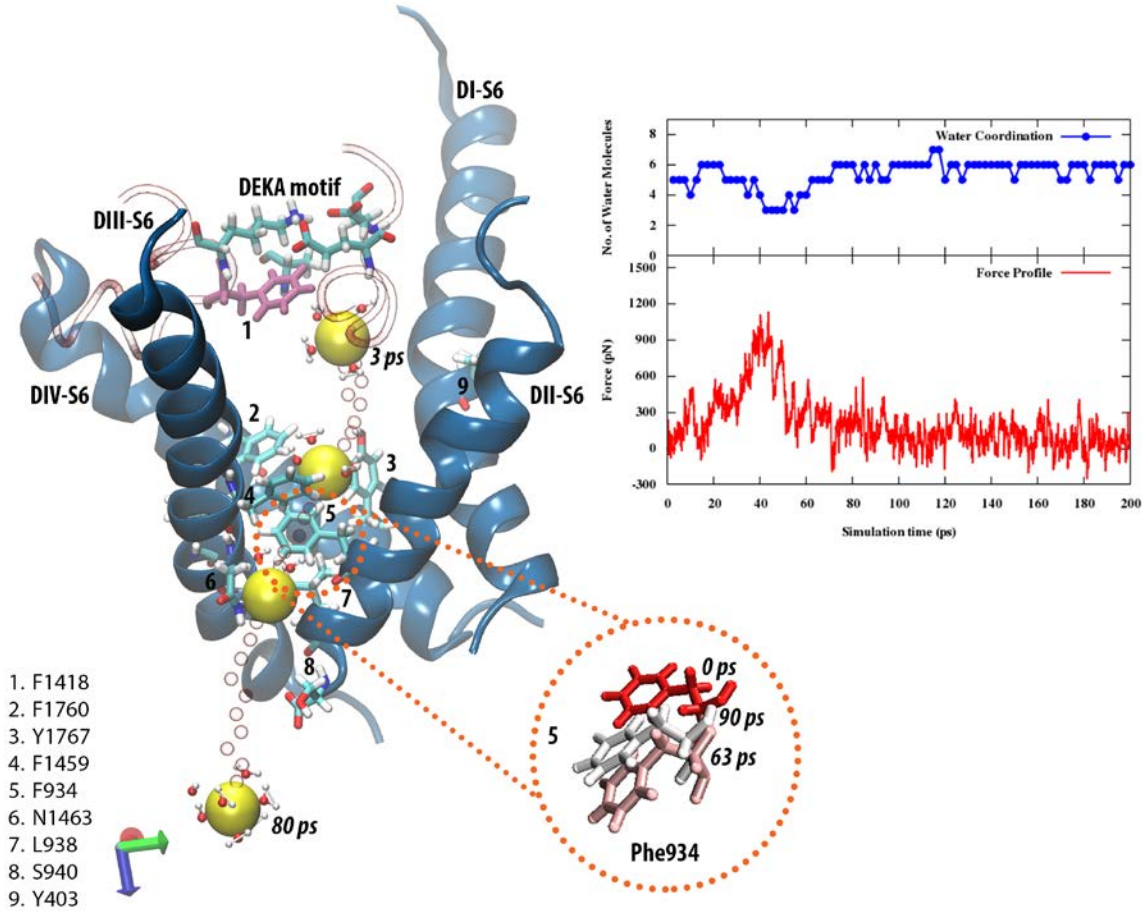

Figure S8. The pulling of Na+ ion out of the central cavity of the $Na_v1.5$ model in the snap3 through pathway 2. The 3D representation on the left describes that the Na+ ion (shown as a yellow VDW sphere) trapped near the DEKA motif at the central cavity of the ion channel exits through the S6 helices (shown as blue ribbons) of the domains, DIII and DIV. The ion, under the influence of external force, passes through a number of hydrophobic residues (shown as sticks and listed in the figure) and finally released by disruption of H-bonds between V1337 and C1341 residues (shown within rectangular box) and later via the short S4/S5 helix of DII. The positions of the ion surrounded by water molecules at different timescales (*3 ps, 33 ps, 58 ps and 68 ps*) during the SMD simulation are shown as VDW spheres in yellow and the positions of the ions along each step until the exit are shown as smaller CPK spheres in red. The corresponding force profile for the pulling of the ion and the numbers of water molecules surrounding the ions throughout this trajectory are shown in the bottom and the upper panels, respectively, of the right-side figure.

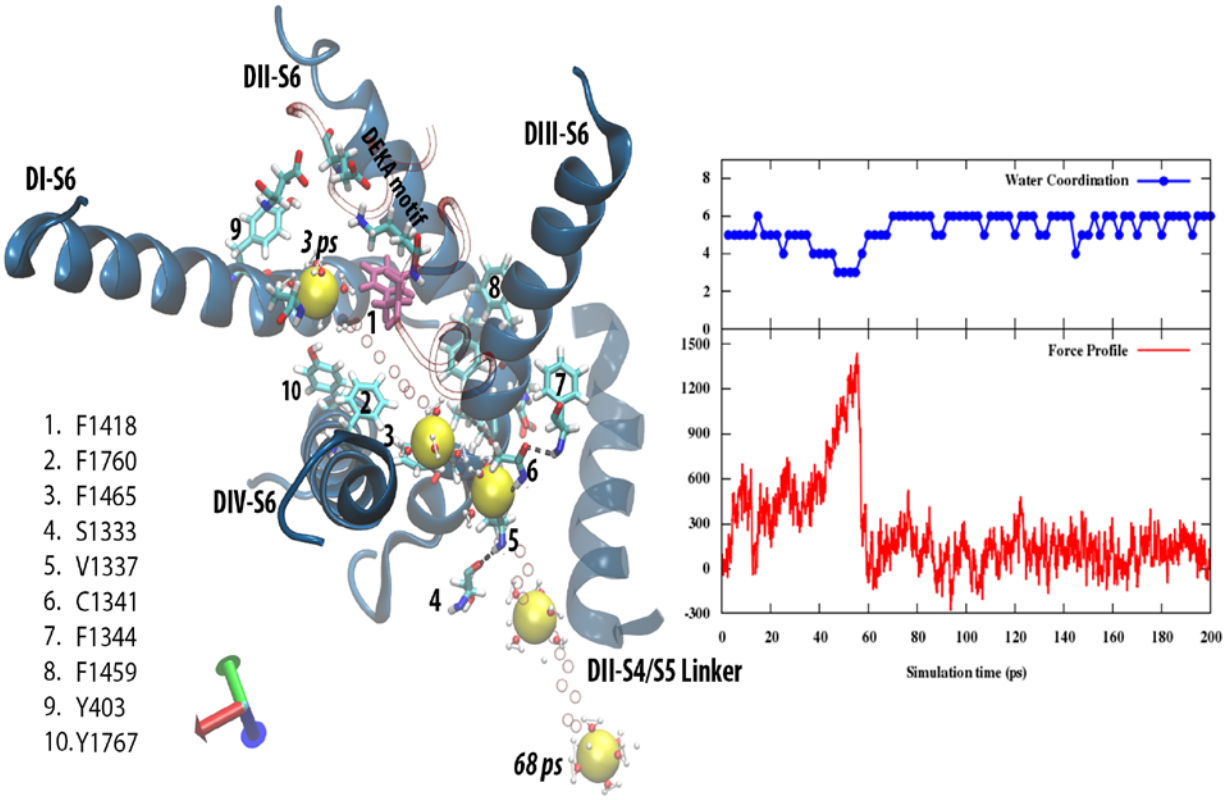

Figure S9. The pulling of Na+ ion out of the central cavity of the $Na_v1.5$ model in the snap7 through pathway 2. The 3D representation on the left describes that the Na+ ion (shown as a yellow VDW sphere) trapped near the DEKA motif at the central cavity of the ion channel exits through the S6 helices (shown as blue ribbons) of the domains, DIII and DIV. The ion, under the influence of external force, passes through a number of hydrophobic residues (shown as sticks and listed in the figure) and finally released by disruption of H-bonds between V1337 and C1341 residues (shown within rectangular box) and later via the short S4/S5 helix of DII. The positions of the ion surrounded by water molecules at different timescales (*3 ps, 33 ps, 63 ps and 78 ps*) during the SMD simulation are shown as VDW spheres in yellow and the positions of the ions along each step until the exit are shown as smaller CPK spheres in red. The corresponding force profile for the pulling of the ion and the numbers of water molecules surrounding the ions throughout this trajectory are shown in the bottom and the upper panels, respectively, of the right-side figure.

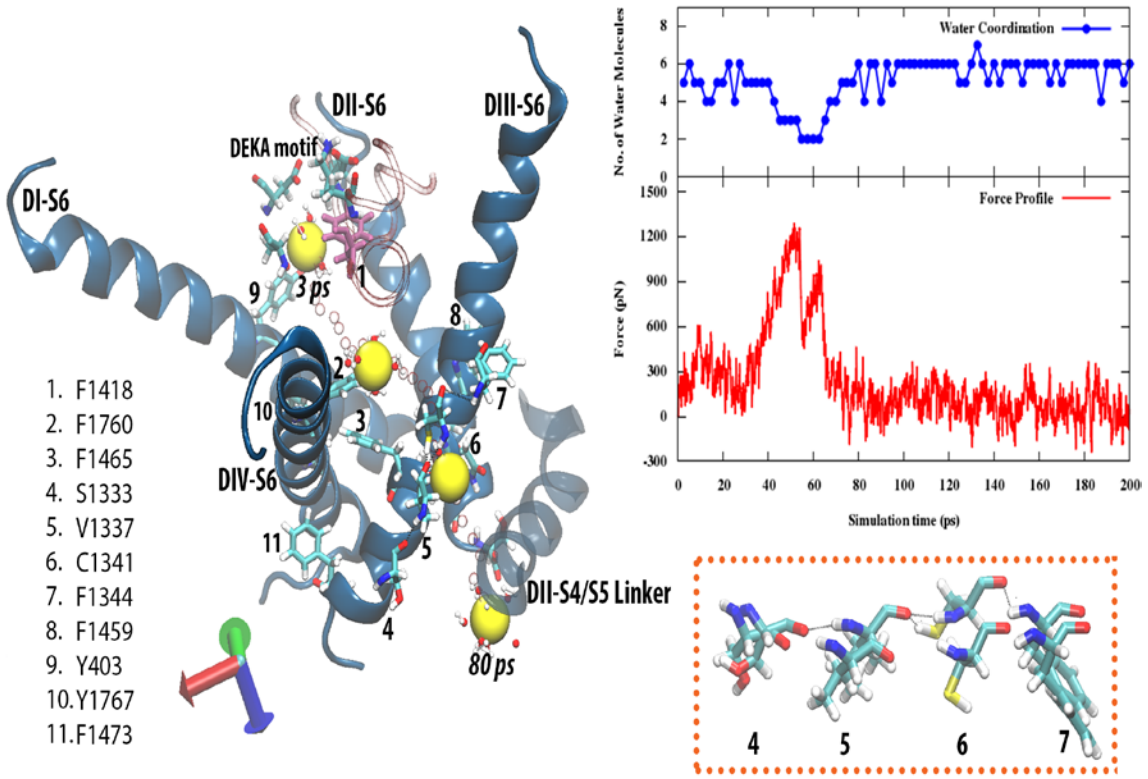

Figure S10. The force profiles for the pulling of Na+ ion out of the central cavity of the $Na_v1.5$ model in the snap5 through pathway 1 (a) and pathway 2 (b).

(a)

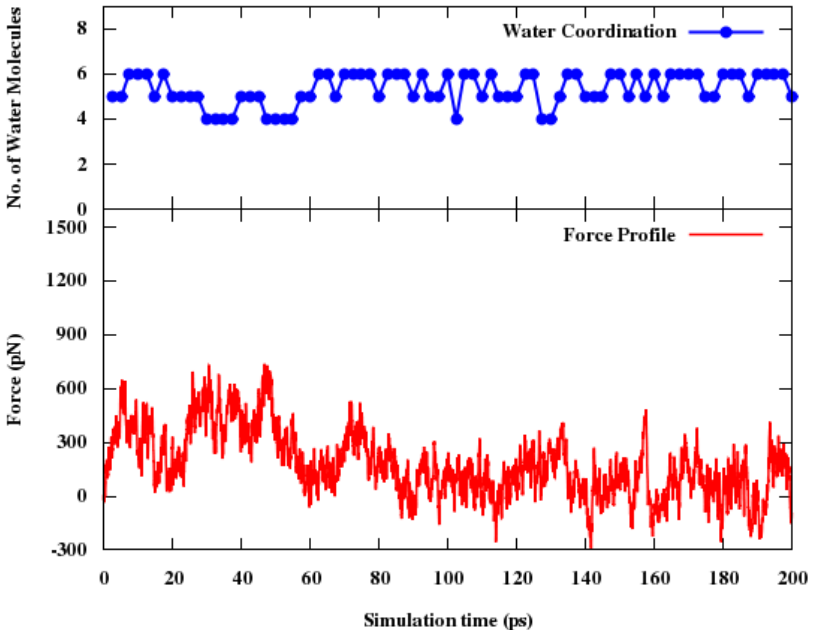

(b)

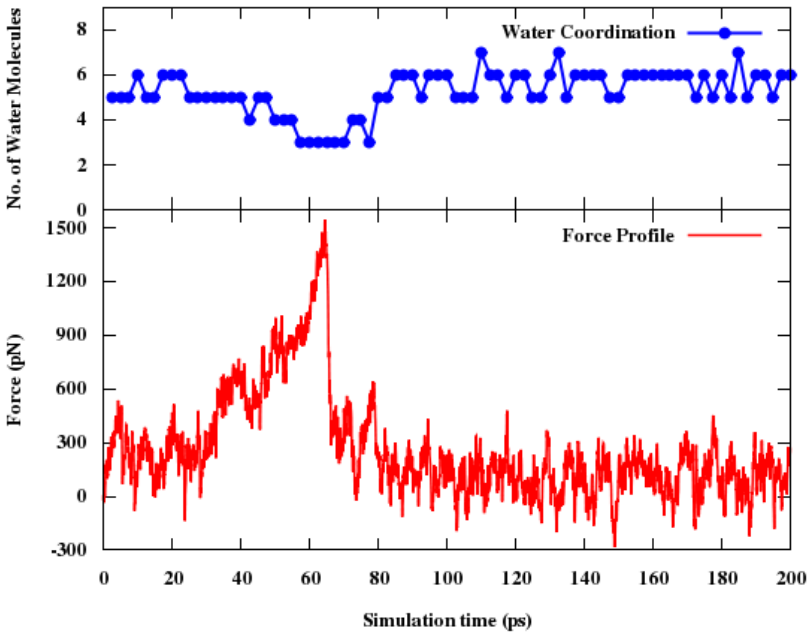

Figure S11: Exchange of water through pathway 1 and pathway 2 identified through SMD simulations. The upper panel shows the blockade of water molecules by the gating residues along pathway 1 (left) and pathway 2 (right) at the initial step of SMD simulation of snap1; whereas, the structures in the bottom panel shows the water passing through the channel, as soon as the gating residues along the two pathways change conformations.

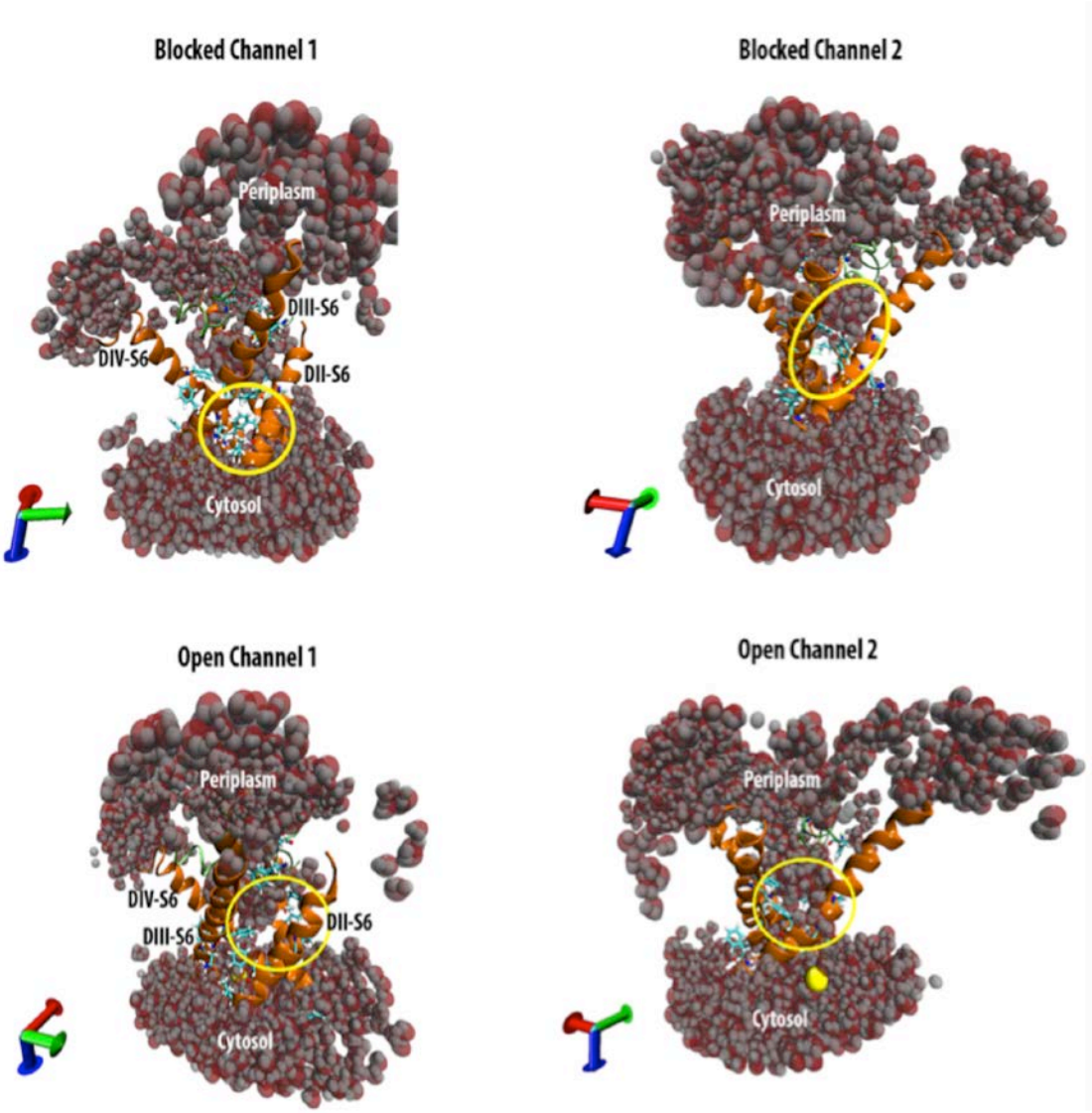

HNav1.5 Model validation against some known mutations

As reported in the literature, the first step of the depolarization-induced opening of VGSCs involves an outward movement of the S4 helices in the VSD domains with respect to S1-S3 helices [36]. This step is facilitated by the presence of a high propensity of positively charged R/K residues at the S4 helices, which are stabilized by their salt-bridge interactions with the negatively charged residues on S1-S3 in an inactive state of the channel. These positively charged residues on the S4 helices are denoted in the literature as the gating charge transfer center (GCTC) [37,38].

Mutating some of the positively charged residues in the GCTC has been reported to be responsible for some severe forms of cardiac diseases [39]. For instance, R222Q and R225W mutant forms have been found to be related to cardiac arrhythmias and dilatation of cardiac chambers [39]. A recent patch-clamp experiment-based study[40] concluded that the R222Q and the R225W mutations also lead to ion leakage in the VSD, i.e., the VSDI domain gains a pore conducting function. Thus, the salt bridge interactions between the residues on S4 helix and S1-S3 helices in the VSDs are important for the stability of the structure.

In our model, R222 is stabilized by the formation of a strong salt-bridge interaction with E161 (Figure S12). On the other hand, R225, which forms only a weak interaction with

E161 in our model, is oriented towards the central axis of VSDI, thus possibly creating an energy barrier for the passage of ions in this direction. This data is in accordance with the results reported by Moreau et. al.[40], which showed that mutating R225W results in a more profound effect on the conductance of the VSDI domain, compared to mutating the R222Q residue. The main conclusion from that study is that a leaking VSD domain, resulting from the R222Q and the R225W mutations, creates a pathway for ions to pass through this VSD domain. It is also possible that a rather complex mechanism, involving the coupling between the S4 and the pore helical movements, may also exist, which is yet to be established.

Figure S12. A carton representation of the VSDI domain of the hNa$_v$1.5 model. The S4 helix is shown in green whereas other helices (S1-S3) are shown in sky-blue color. As we can see, R222 forms a salt bridge with E161 whereas R225 points toward the central axis of the VSD, explaining the profound effect of mutating these residues on the gating current of hNa$_v$1.5. The lower cluster of interacting residues, Y168, D179 and R225 form a septum preventing the outward movement of waters and ions through the VSD pore.

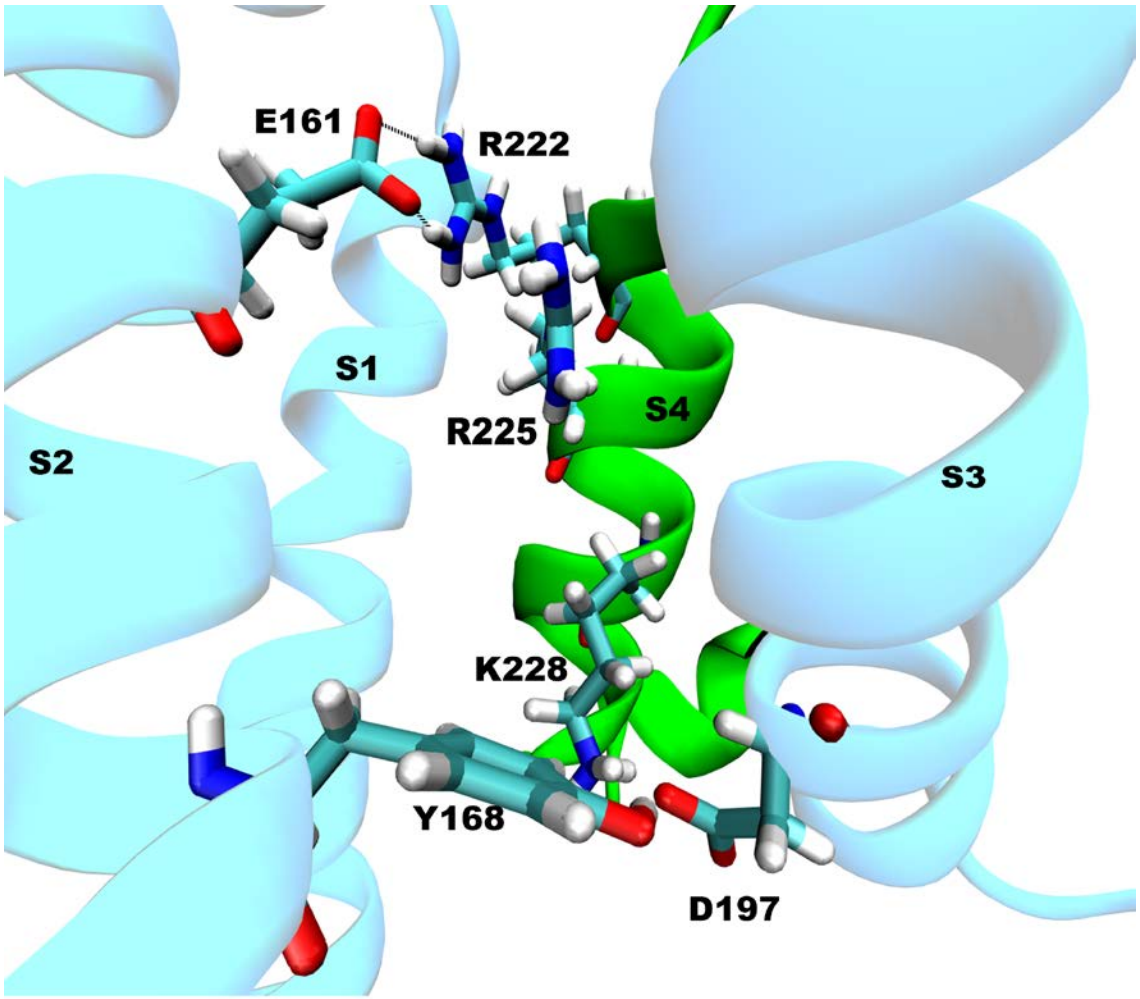

In addition to the obstruction to the ion passage created by R225 against ions, we also noted that an additional septum created by a stable rotamer of Y168 on S2 blocks the VSDI domain from below, preventing water and ion permeation from inside to the outside of the channel. This Y168 rotamer is stabilized by H-bonding with D197 residue on S3 that is also stabilized by K228 on S4. As shown in Figure S12, Y168 is bonded to D197 that is bonded to K228. The loss of this H-bond network formed by Y168, as in the case of the Y168F mutation, disturbs the gating current of $hNa_v1.5$ as previously reported in an experimental study by Amarouch et al [41]. We also noted that Y168 does not form H-bond with R225, again in accordance with experimental and computational results reported by Amarouch et.al. [41]. In that study, the Y168-R225 H-bond was only observed in the I141V mutant of $hNa_v1.5$, not in the wild type form.

References:

1. Magrane M, Consortium U. UniProt Knowledgebase: a hub of integrated protein data. *Database.* January 1, 2011 2011;2011.
2. Wilkins MR, Gasteiger E, Bairoch A, et al. Protein identification and analysis tools in the ExPASy server. *Methods Mol Biol.* 1999;112:531-552.
3. Artimo P, Jonnalagedda M, Arnold K, et al. ExPASy: SIB bioinformatics resource portal. *Nucleic Acids Res.* Jul 2012;40(Web Server issue):W597-603.
4. Roy A, Kucukural A, Zhang Y. I-TASSER: a unified platform for automated protein structure and function prediction. *Nat. Protocols.* 04//print 2010;5(4):725-738.
5. Payandeh J, Gamal El-Din TM, Scheuer T, Zheng N, Catterall WA. Crystal structure of a voltage-gated sodium channel in two potentially inactivated states. *Nature.* Jun 7 2012;486(7401):135-139.
6. Mahdavi S, Kuyucak S. Molecular dynamics study of binding of micro-conotoxin GIIIA to the voltage-gated sodium channel Na(v)1.4. *PLoS One.* 2014;9(8):e105300.
7. Yang Y, Dib-Hajj SD, Zhang J, et al. Structural modelling and mutant cycle analysis predict pharmacoresponsiveness of a Na(V)1.7 mutant channel. *Nat Commun.* 2012;3:1186.
8. Tikhonov DB, Zhorov BS. Sodium channel activators: model of binding inside the pore and a possible mechanism of action. *FEBS Lett.* Aug 15 2005;579(20):4207-4212.
9. Ramos E, O'Leary M E. State-dependent trapping of flecainide in the cardiac sodium channel. *The Journal of physiology.* Oct 1 2004;560(Pt 1):37-49.
10. Sokolov S, Peters CH, Rajamani S, Ruben PC. Proton-dependent inhibition of the cardiac sodium channel Nav1.5 by ranolazine. *Front. Pharmacol.* 2013;4:78.
11. Chung S-H, Anderson OS, Krishnamurthy VV. *Biological membrane ion channels: dynamics, structure, and applications.* Springer Science & Business Media; 2007.
12. Wang C, Chung BC, Yan H, Lee SY, Pitt GS. Crystal structure of the ternary complex of a NaV C-terminal domain, a fibroblast growth factor homologous factor, and calmodulin. *Structure.* Jul 3 2012;20(7):1167-1176.
13. Sarhan MF, Tung CC, Van Petegem F, Ahern CA. Crystallographic basis for calcium regulation of sodium channels. *Proc Natl Acad Sci U S A.* Feb 28 2012;109(9):3558-3563.
14. Xu D, Zhang Y. Improving the physical realism and structural accuracy of protein models by a two-step atomic-level energy minimization. *Biophys J.* Nov 16 2011;101(10):2525-2534.
15. Smith TF, Waterman MS. Identification of common molecular subsequences. *J Mol Biol.* Mar 25 1981;147(1):195-197.

16. Pettersen EF, Goddard TD, Huang CC, et al. UCSF Chimera--a visualization system for exploratory research and analysis. *Journal of computational chemistry.* Oct 2004;25(13):1605-1612.
17. Zhang J, Liang Y, Zhang Y. Atomic-level protein structure refinement using fragment-guided molecular dynamics conformation sampling. *Structure.* Dec 7 2011;19(12):1784-1795.
18. Chu M, Desvoyes B, Turina M, Noad R, Scholthof H. Structure validation by C geometry: φ, and C deviation. *Proteins.*50:437-450.
19. Wu EL, Cheng X, Jo S, et al. CHARMM-GUI Membrane Builder toward realistic biological membrane simulations. *Journal of computational chemistry.* Oct 15 2014;35(27):1997-2004.
20. Huang J, MacKerell AD, Jr. CHARMM36 all-atom additive protein force field: validation based on comparison to NMR data. *Journal of computational chemistry.* Sep 30 2013;34(25):2135-2145.
21. Davidchack RL, Handel R, Tretyakov MV. Langevin thermostat for rigid body dynamics. *The Journal of chemical physics.* Jun 21 2009;130(23):234101.
22. Yoo J, Aksimentiev A. Improved parametrization of Li+, Na+, K+, and Mg2+ ions for all-atom molecular dynamics simulations of nucleic acid systems. *The Journal of Physical Chemistry Letters.* 2011;3(1):45-50.
23. Phillips JC, Braun R, Wang W, et al. Scalable molecular dynamics with NAMD. *Journal of computational chemistry.* 2005;26(16):1781-1802.
24. Lu H, Schulten K. The Key Event in Force-Induced Unfolding of Titin's Immunoglobulin Domains. *Biophys J.* 7// 2000;79(1):51-65.
25. Colizzi F, Perozzo R, Scapozza L, Recanatini M, Cavalli A. Single-Molecule Pulling Simulations Can Discern Active from Inactive Enzyme Inhibitors. *J Am Chem Soc.* 2010/06/02 2010;132(21):7361-7371.
26. Giorgino T, De Fabritiis G. A High-Throughput Steered Molecular Dynamics Study on the Free Energy Profile of Ion Permeation through Gramicidin A. *J. Chem. Theory Comput.* 2011/06/14 2011;7(6):1943-1950.
27. Izrailev S, Stepaniants S, Balsera M, Oono Y, Schulten K. Molecular dynamics study of unbinding of the avidin-biotin complex. *Biophys J.* 1997;72(4):1568-1581.
28. Kalyaanamoorthy S, Chen Y-PP. A steered molecular dynamics mediated hit discovery for histone deacetylases. *PCCP.* 2014;16(8):3777-3791.
29. Kóňa J, Minozzi M, Torre V, Carloni P. A gate mechanism indicated in the selectivity filter of the potassium channel KscA. *Theor. Chem. Acc.* 2007// 2007;117(5):1121-1129.
30. Kosztin D, Izrailev S, Schulten K. Unbinding of retinoic acid from its receptor studied by steered molecular dynamics. *Biophys J.* 1999;76(1 I):188-197.
31. Mahdavi S, Kuyucak S. Mechanism of Ion Permeation in Mammalian Voltage-Gated Sodium Channels. *PLoS ONE.* 2015;10(8):e0133000.
32. Anwar-Mohamed A, Barakat KH, Bhat R, et al. A human ether-a-go-go-related (hERG) ion channel atomistic model generated by long supercomputer molecular dynamics simulations and its use in predicting drug cardiotoxicity. *Toxicology letters.* Nov 4 2014;230(3):382-392.

33. Salomon-Ferrer R, Case DA, Walker RC. An overview of the Amber biomolecular simulation package. *Wiley Interdisciplinary Reviews: Computational Molecular Science.* 2013;3(2):198-210.
34. Su PC, Tsai CC, Mehboob S, Hevener KE, Johnson ME. Comparison of radii sets, entropy, QM methods, and sampling on MM-PBSA, MM-GBSA, and QM/MM-GBSA ligand binding energies of F. tularensis enoyl-ACP reductase (FabI). *Journal of computational chemistry.* Sep 30 2015;36(25):1859-1873.
35. Miller BR, 3rd, McGee TD, Jr., Swails JM, Homeyer N, Gohlke H, Roitberg AE. MMPBSA.py: An Efficient Program for End-State Free Energy Calculations. *Journal of chemical theory and computation.* Sep 11 2012;8(9):3314-3321.
36. Yarov-Yarovoy V, DeCaen PG, Westenbroek RE, et al. Structural basis for gating charge movement in the voltage sensor of a sodium channel. *Proceedings of the National Academy of Sciences of the United States of America.* Jan 10 2012;109(2):E93-102.
37. Gosselin-Badaroudine P, Delemotte L, Moreau A, Klein ML, Chahine M. Gating pore currents and the resting state of Nav1.4 voltage sensor domains. *Proceedings of the National Academy of Sciences of the United States of America.* Nov 20 2012;109(47):19250-19255.
38. Moreau A, Gosselin-Badaroudine P, Chahine M. Biophysics, pathophysiology, and pharmacology of ion channel gating pores. *Frontiers in pharmacology.* 2014;5:53.
39. Song W, Shou W. Cardiac sodium channel Nav1.5 mutations and cardiac arrhythmia. *Pediatric cardiology.* Aug 2012;33(6):943-949.
40. Moreau A, Gosselin-Badaroudine P, Boutjdir M, Chahine M. Mutations in the Voltage Sensors of Domains I and II of Nav1.5 that are Associated with Arrhythmias and Dilated Cardiomyopathy Generate Gating Pore Currents. *Frontiers in pharmacology.* 2015;6:301.
41. Amarouch MY, Kasimova MA, Tarek M, Abriel H. Functional interaction between S1 and S4 segments in voltage-gated sodium channels revealed by human channelopathies. *Channels.* 2014;8(5):414-420.